Preventing Chaotic Motion in Tapping-Mode Atomic Force Microscope

Kleber dos Santos Rodrigues · **José Manoel Balthazar** ·
Angelo Marcelo Tusset · **Bento Rodrigues de Pontes Jr.** ·
Átila Madureira Bueno

Abstract During the last 30 years the Atomic Force
Microscopy became the most powerful tool for surface prob-
ing in atomic scale. The Tapping-Mode Atomic Force Micro-
scope is used to generate high quality accurate images of
the samples surface. However, in this mode of operation the
microcantilever frequently presents chaotic motion due to
the nonlinear characteristics of the tip-sample forces inter-
actions, degrading the image quality. This kind of irregu-
lar motion must be avoided by the control system. In this
work, the tip-sample interaction is modelled considering the
Lennard-Jones potentials and the two-term Galerkin aprox-
imation. Additionally, the State Dependent Ricatti Equation
and Time-Delayed Feedback Control techniques are used in
order to force the Tapping-Mode Atomic Force Microscope
system motion to a periodic orbit, preventing the microcan-
tilever chaotic motion.

K. S. Rodrigues
Departamento de Engenharia Mecânica, Escola
de Engenharia de São Carlos - EESC, Universidade de São
Paulo - USP, São Paulo, Brazil
e-mail: kleber_sr@hotmail.com

J. M. Balthazar
Departamento de Estatística, Matemática Aplicada e
Computação - DEMAC, Universidade Estadual
Paulista - UNESP, São Paulo, Brazil
e-mail: jmbaltha@rc.unesp.br

A. M. Tusset
Departamento Academico de Engenharia Eletrônica - DAELE,
Campus de Ponta Grossa, Universidade Tecnológica
Federal do Paraná - UTFPR, Ponta Grossa, Brazil
e-mail: a.m.tusset@gmail.com

B. R. de Pontes Jr.
Departamento de Engenharia Mecânica, Faculdade de
Engenharia de Bauru - FEB, Universidade Estadual
Paulista - UNESP, São Paulo, Brazil
e-mail: brpontesjr@hotmail.com

A. M. Bueno (✉)
Departamento de Engenharia de Controle e Automação - ECA,
Campus de Sorocaba, Universidade Estadual
Paulista - UNESP, Sorocaba, Brazil
e-mail: atila@sorocaba.unesp.br

1 Introduction

The Atomic Force Microscope (AFM) is a powerful tool for
atomic scale surface investigation. Its applications include
manipulation of carbon nanotubes, DNA studies, imaging of
atomic scale surfaces, nanoelectronics, and others (Rützel
et al. 1948). The AFM system consists of a microcantilever
with a sharp tip at its free end. The tip-sample interaction
forces are modulated in the microcantilever motion, that is
detected by the deflection of a laser beam that incides on a
photodetector (Fig. 1) (Balthazar et al. 2013; Nozaki et al.
2013).

The AFM operates in simple contact, noncontact and inter-
mittent (tapping) contact modes. In the tapping mode, the
microcantilever is deliberately vibrated very close to the sam-
ple surface, and near its resonant frequency, softly tapping the
sample. In this case, the influence of intermolecular forces
frequently lead the microcantilever to a characteristic nonlin-
ear motion (Jalili and Laxminarayana 2004; Bhushan 2004;
Morita et al. 2009; Zhong et al. 1993).

In the TM-AFM, the chaotic motion may occur during the
transtion from noncontact mode to the tapping mode (Hu and
Raman 2006). Besides, a complicating factor related to the
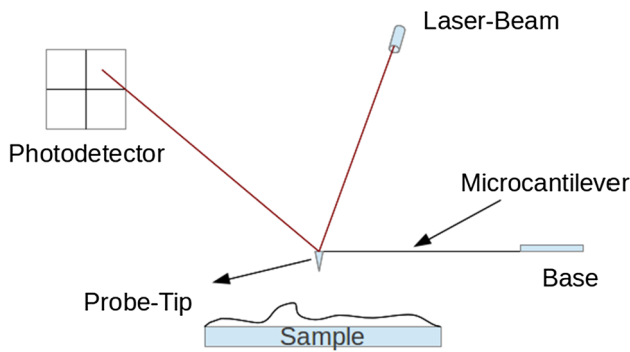TM-AFM motion is due to the impact (contact) between tip

Fig. 1 AFM simplified schematic diagram

and sample, and, in most cases, the tip-surface interaction is represented by a generic tip-surface-interaction potential avoiding more detailed and computationally expensive models (Rützel et al. 1948).

In Zhao and Dankowicz (2006) the AFM tip-sample interaction is modeled a mass-spring-damper system, and the attractive and repulsive forces are represented as negative and positive linear spring coefficients.

In Stark et al. (2004), the Derjaguin–Muller–Toporov theory is used to represent the contact between the tip and the sample surface, and in Jalili and Laxminarayana (2004), different modelling approaches are presented.

Additionally, in Babahosseini et al. (2009) and Misra et al. (2008) different control strategies are used, improving the AFM performance. According to Haeri and Khademian (2006), many methods have been applied for the synchronization of chaotic systems. Some refereces of synchronization of chaotic systems can be found where periodic parametric perturbation methods are used in drive-response synchronization, adaptive control method, sliding mode, backstepping control, and H_∞ (Suykens et al. 1997; Astakhov et al. 1997; Blazejczyk-Okolewska et al. 2001; Yang et al. 1999; Wang et al. 2004; CHUA et al. 1996; Liao 1998; Lian et al. 2002; Wu et al. 1996; Fang et al. 1999; Yin et al. 2002; YU and SONG 2001; Wang and Ge 2001; Lü and Zhang 2001).

In Nozaki et al. (2013) the noncontact mode of operation is considered, and te microcantilever is modelled as a nonlinear spring-mass system. In the noncontact mode the AFM operates in a long-range distance from the sample, and the Van-der-Waals forces are predominant. In this case, the Optimal Linear Feedback Control (OLFC) and the State Dependent Riccati Equation (SDRE) control techniques are used in order to prevent chaotic motion, leading the AFM to a periodic motion.

In Rützel et al. (1948) the TM-AFM tip-sample interaction model considers the Lennard-Jones potentials, leading to a nonlinear partial differential equation. Additionally, simplified equations of motion based on Galerkin discretization are obtained. In Hu and Chen (2008) bifurcations and chaos

are numerically investigated for the one-term and two-term Galerkin truncation.

In Balthazar et al. (2013) the TM-AFM mode of operation is studied. The microcantilever is modelled as a nonlinear lumped parameter mass-spring-damper system, the tip-sample interaction forces are obtained from the Lennard-Jones potential, and the attraction basins are numerically investigated. Additional numerical simulations show the existence of chaotic behavior for some regions in the parameter space. In order to prevent chaotic motion the OLFC and the Time-Delayed Feedback Control (TDFC) control techniques are compared.

In this work the microcantilever beam is aproximated by an Euler–Bernoulli beam, as in Rützel et al. (1948), the tip-sample interation forces are described by the Lennard-Jones potentials, and only the first mode of vibration is considered. Numerical simulations are performed showing the onset of chaotic motion in the microcantilever displacement. The chaotic vibration is analysed by means of phase portraits, Fast-Fourier Transform, Poincaré section and Lyapunov exponents plots. In order to prevent the microcantilever chaotic motion two control techniques are applied, namely, the SDRE and the TDFC technique. Both control techniques synchronize the system to a periodic orbit obtained with the Harmonic Balance Method (HBM).

The paper is organized as follows, in Sect. 2 the mathematical model of the AFM is determined. In Sect. 3 the numerical simulations results are shown. In Sect. 4 the periodic solution is obtained. In Sect. 5 the control methods are implemented and simulations results are shown, and in Sect. 6 the concluding remarks are presented.

2 AFM Mathematical Model

Microcantilevers often use lumped parameters models and Lennard-Jones potential. On the other hand, in Rützel et al. (1948) an elastic-Bernoulli–Euller model for straight, rectangular cross-section microcantilevers were used, leading to nonlinear and non-autonomous partial differential equations of motion. In Hu and Chen (2008), the one-term Galerkin truncation is considered, leading to the nondimensional mathematical model of the TM-AFM, given by:

$$\ddot{y} = -d_1\dot{y} - y + B_1 + \frac{C_{11}}{(1 - y - \eta\sin(\Omega t))^8}$$
$$+ \frac{C_{12}}{(1 - y - \eta\sin(\Omega t))^2} + \eta\Omega^2 E_1\sin(\omega t) \quad (1)$$

where y represents the nondimensional positive displacement of the tip, and η represents the ratio between the piezoelectric actuator excitation and the tip-sample equilibrium gap.

Defining the state variables as $\mathbf{x} = \begin{bmatrix} x_1 & x_2 \end{bmatrix}^T = \begin{bmatrix} y & \dot{y} \end{bmatrix}^T$, the system of Eq. 1 is transformed into state space form as follows:

$$\dot{x}_1 = x_2$$
$$\dot{x}_2 = d_1 x_2 + x_1 - B_1$$
$$- \frac{C_{11} + C_{12}(1 - x_1 - \eta \sin(\Omega t))^6}{(1 - x_1 - \eta \sin(\Omega t))^8}$$
$$+ \eta \Omega^2 E_1 \sin(\omega t). \tag{2}$$

Additionally, it is assumed that the excitation frequency is close to the natural frequency of the microcantilever, $\Omega = 1$, and the other coefficients of Eq. 2 are given by: $d_1 = 0,01$, $B_1 = -0.148967$, and $E_1 = 1.57367$.

3 Numerical Simulations Results

The numerical simulations performed with the system of Eq. 2 are shown. The Fig. 2 shows the bifurcation diagram of the microcantilever tip displacement as a function of the nondimensional amplitude η. It can be noticed that for $\eta \approx 0.21$ a discontinuity occurs in the tip displacement amplitude, it can be explained by the characteristics of Lennard-Jones potentials. When the excitation amplitude increases, for $\eta \approx 0.613$, the period-1 motion becomes a period-2 motion. After this period doubling, for $\eta > 10.99$ the system becomes chaotic, with indications of some period windows in the chaotic region. The analysis of Fig. 3 shows that for $\eta > 0.99$ the TM-AFM motion becomes chaotic.

The Lyapunov exponents are determined by the Jacobian algorithms (Wolf et al. 1985), and are shown in Fig. 3, for $\eta = 0.99$. The existence of positive Lyapunov exponent ($\lambda_1 = 0.062205$) indicates the onset of chaotic behavior. Additionally, Fig. 4a shows the phase portrait with chaotic
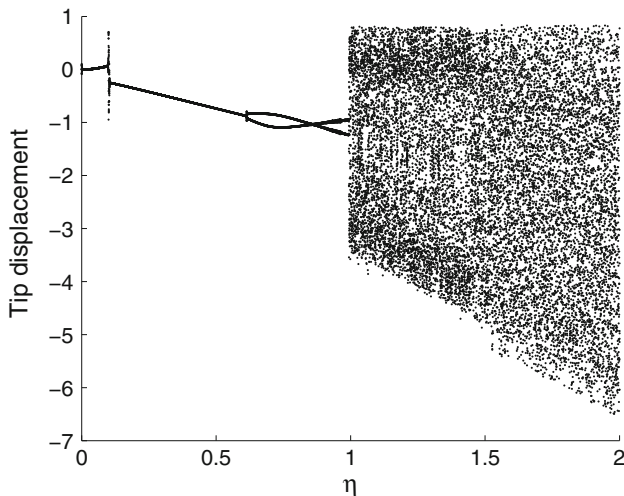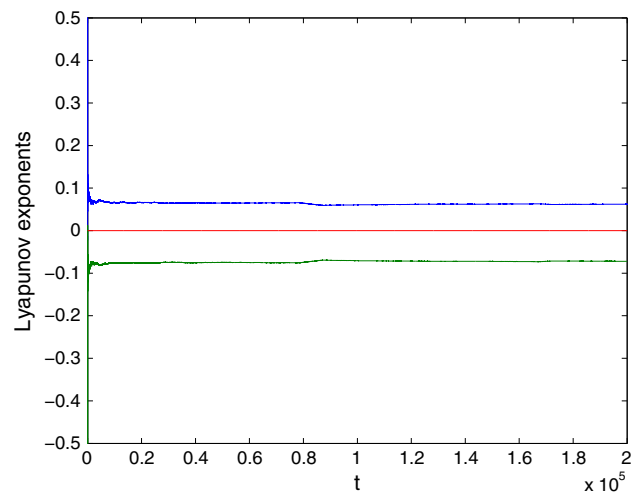
Fig. 3 Lyapunov exponents ($\lambda_1 = 0.062205$), for $\eta = 0.99$

behavior and the Fig. 4b shows the Poincaré section with the presence of a strange attractor. Figure 4c, d shows the frequency spectrum and time response of the system, respectively. In Fig. 4c, the numerous resonance peaks indicate the existence of chaotic behavior on the microcantilever displacement.

4 Periodic Solutions

The aim of this section is to find periodic solutions for the system of Eq. 2. According to Guran and Rand (1997), an unperturbed system that presents chaotic behavior can be considered strongly nonlinear, and traditional methods such as the multiple scales and average methods become unsuitable. In this section, two different approaches for searching periodic solutions are presented, the HBM (Nayfeh and Mook 1995), and a parameter modification technique.

4.1 The Harmonic Balance Method

The main idea of the HBM is to consider a periodic solution of 2 in the following form (Nayfeh and Mook 1995):

$$y = \alpha_0 + \alpha_1 \cos(\omega t) + \beta_1 \sin(\omega t) + \alpha_2 \cos(2\omega t)$$
$$+ \beta_2 \sin(2\omega t) + \cdots \tag{3}$$

Considering only the first harmonic therms of Eq. 3, results:

$$y = \alpha_0 + \alpha_1 \cos(\omega t) + \beta_1 \sin(\omega t) \tag{4}$$

and applying the initial conditions, $t_0 = 0$, $y(0) = y_0$ and $\dot{y}(0) = \dot{y}_0$, the coefficients can be determined by:

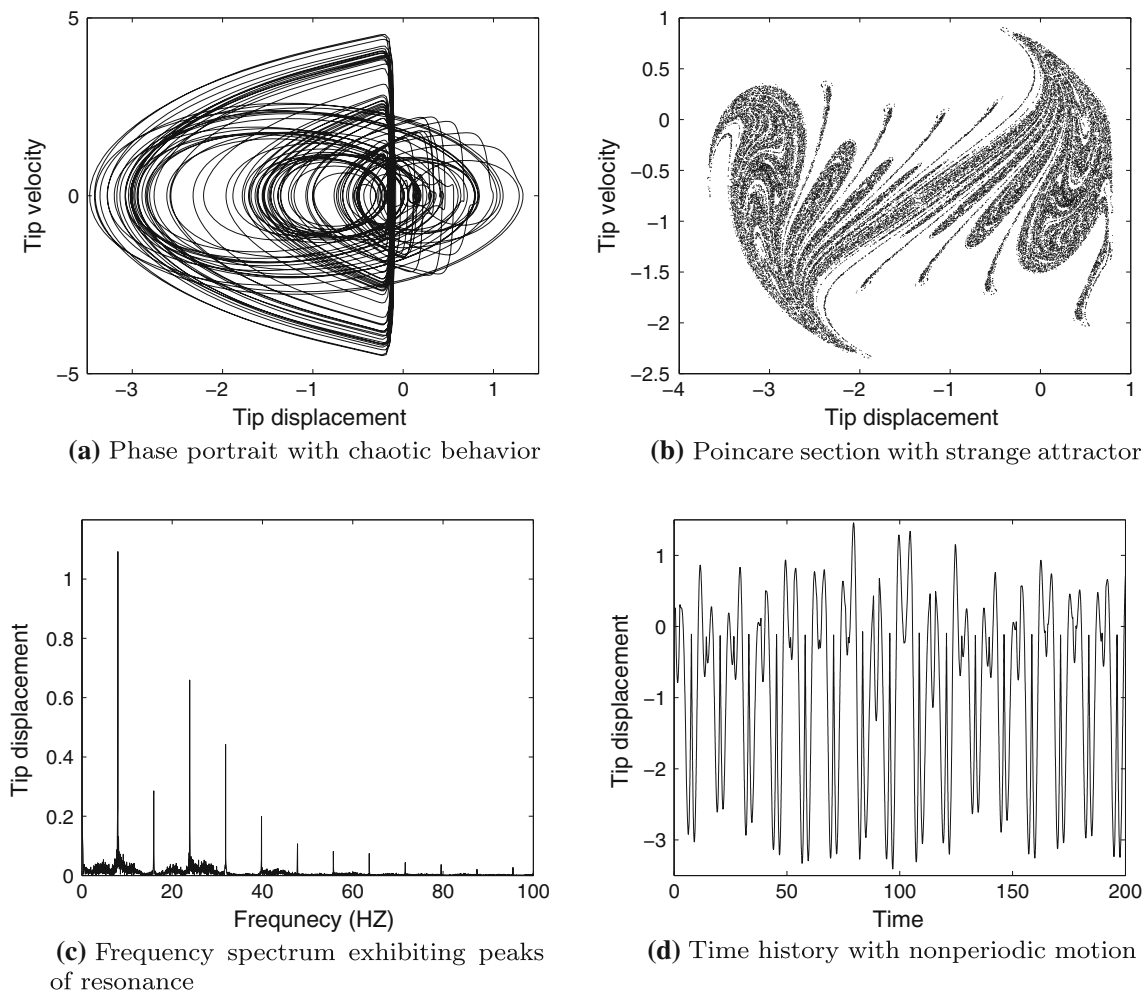$$\alpha_0 + \alpha_1 = y_0 \tag{5}$$
$$\beta_1 = \dot{y}_0 \tag{6}$$

Fig. 2 Bifurcation diagram of the tip displacement vesus η

(a) Phase portrait with chaotic behavior

(b) Poincare section with strange attractor

(c) Frequency spectrum exhibiting peaks of resonance

(d) Time history with nonperiodic motion

Fig. 4 Microcantilever behavior

Considering the Eqs. 5 and 6 and replacing Eq. 4 into Eq. 2, for $t = 0$ results that $\cos(\omega t) = 1$ and $\sin(\omega t) = 0$ and the following constant terms are determined:

$$-\alpha_0 + B_1 = 0 \tag{7}$$

and for $y(0) = 0.2$ and $\dot{y} = 0$ a periodic solution is found and is given by:

$$y = -0.148967 + 0.348967\cos(t) \tag{8}$$

The phase portrait and the time history of the harmonic balance solution are shown in Fig. 5.

The periodic solution found in this section is going to be used as the target curve the control system must track.

4.2 System with Periodic Motion and Different Parameters

This section presents the system of Eq. 2, considering another set of parameters $d_1 = 0.01$, $\eta = 0.01$, $B_1 = 0.148967$, $C_{11} = -4.59118 \times 10^{-5}$, $C_{12} = 0.149013$ and $E_1 = 50$. In Fig. 6 the simlations results for this system are shown.

As it can be noticed the system presents periodic motion for $900 \leqslant t \leqslant 1000$.

5 Control System Design

In this section presents the SDRE (Fenili and Balthazar 2011) and the TDFC (Pyragas 2002) methods are applied to control the TM-AFM.

5.1 SDRE Design

The SDRE technique is used to force the chaotic amplitude displacement of the TM-AFM to the periodic orbit (Eq. 8) obtained with the HBM. Besides the SDRE controller, a feedfoward compensator is used to track the periodic orbit.

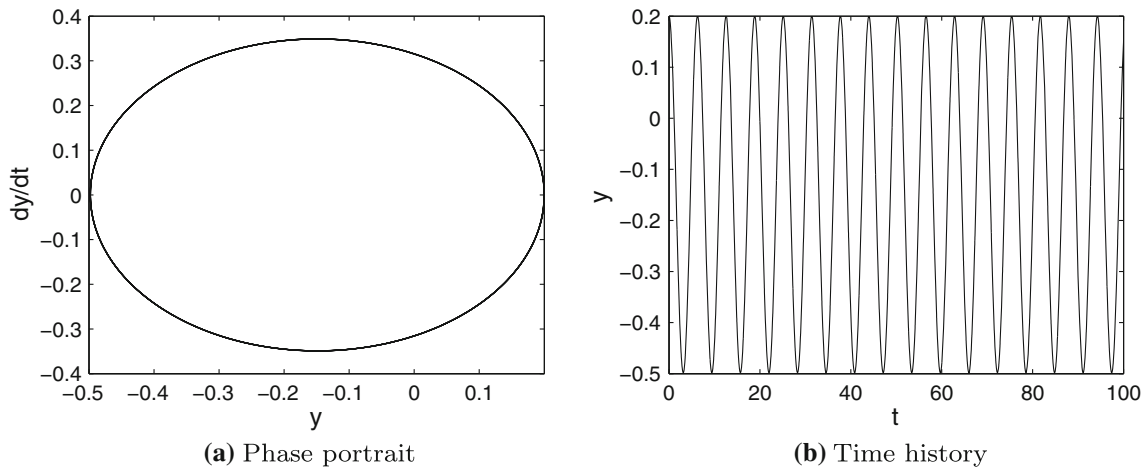The nonlinear system of Eq. 2 can be rewritten in the following form:

(a) Phase portrait

(b) Time history

Fig. 5 Harmonic balance solution

(a) Phase portrait of the system with periodic behavior

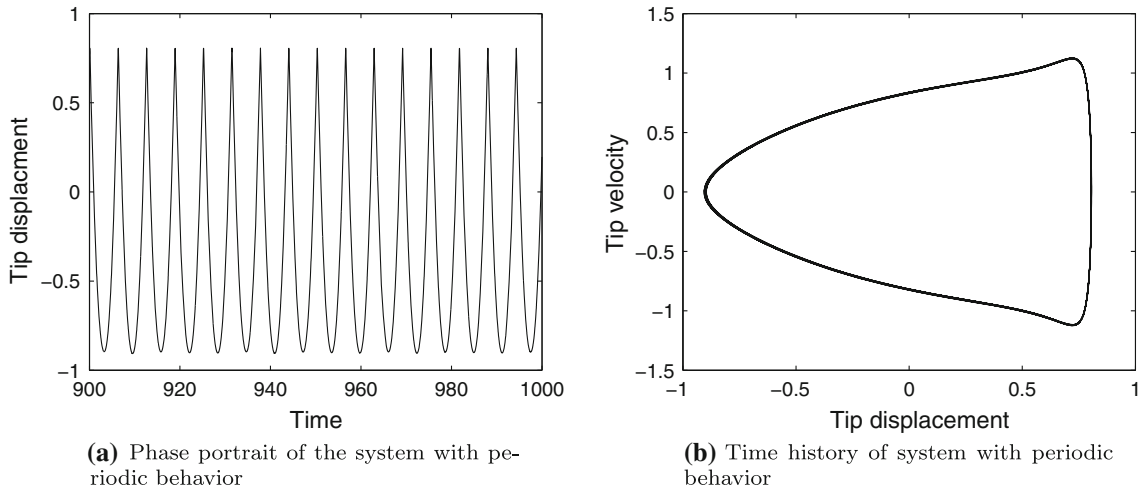**(b)** Time history of system with periodic behavior

Fig. 6 Periodic behavior of the system with new parameters

$$\dot{\mathbf{x}} = \mathbf{A}(\mathbf{x})\mathbf{x} + \mathbf{F} \tag{9}$$

where $\mathbf{x} \in \mathbf{R}^n$ is the state vector, $\mathbf{A} \in R^{n \times n}$ is the state-dependent matrix, $\mathbf{F}$ is the nonlinear vector of the non-state-dependent variables.

If $\mathbf{A}(\mathbf{x}) = \mathbf{A}$, i.e., non-state-dependent, the SDRE method is the optimal solution of the linear quadratic regulator problem performance (LQR control) (Mracek and Cloutier 1998). Considering the control $\mathbf{U}$ the sistem can be written in the following form:

$$\dot{\mathbf{x}} = \mathbf{A}(\mathbf{x})\mathbf{x} + \mathbf{F} + \mathbf{B}\mathbf{U} \tag{10}$$

with

$$\mathbf{U} = \mathbf{u}_f + \mathbf{u} \tag{11}$$

where $\mathbf{B} \in R^{n \times n}$, and $\mathbf{u}$ is the linear state feedback control.

According to Tusset et al. (2013), the feedfoward control is given by:

$$\mathbf{u}_f = -\mathbf{F} \tag{12}$$

Considering the state feedback strategy, the control signal $\mathbf{u}$ is defined by:

$$\mathbf{u} = -\mathbf{R}^{-1}(\mathbf{x})\mathbf{B}^T(\mathbf{x})\mathbf{P}(\mathbf{x}) = -\mathbf{K}(\mathbf{x})\mathbf{e} \tag{13}$$

where $\mathbf{e} = (\mathbf{x} - \mathbf{x}^*)$ is the error from the periodic desired orbit $\mathbf{x}^*$, and $\mathbf{P}(\mathbf{x})$ is the SDRE solution.

The performance measure to be minimized through the SDRE control is given by:

$$J = \int_0^\infty (\mathbf{e}^T \mathbf{Q}(\mathbf{e})\mathbf{e} + \mathbf{u}_r^T \mathbf{R}(\mathbf{u})\mathbf{u}_r) dt \tag{14}$$

where $\mathbf{Q}(\mathbf{x})$ and $\mathbf{R}(\mathbf{x})$ are positive definite matrices, assumed to have constant coefficients.

Transforming the system into state space form results:

$$\dot{x}_1 = x_2$$
$$\dot{x}_2 = -x_1 - dx_2 + F \tag{15}$$

where

$$F = B_1 + \frac{C_{11} + C_{12}(1 - x_1 - \eta \sin(\Omega t))^6}{(1 - y - \eta \sin(\Omega t))^8}$$
$$+ \eta \Omega^2 E_1 \sin(\omega t) \tag{16}$$

Introducing the feedfoward control of Eq. 12 into Eq. 15 results (Shawky et al. 2007):

$$\begin{bmatrix} \dot{x}_1 \\ \dot{x}_2 \end{bmatrix} = \begin{bmatrix} 0 & 1 \\ -1 & -d_1 \end{bmatrix} \begin{bmatrix} x_1 \\ x_2 \end{bmatrix} + \begin{bmatrix} 0 \\ 1 \end{bmatrix} u \tag{17}$$

The origin of the system of Eq. 17 is the equilibrium point, allowing the application of the SDRE control method (Shawky et al. 2007). Where $\mathbf{A} = \begin{bmatrix} 0 & 1 \\ -1 & -d_1 \end{bmatrix}$, $\mathbf{B} = \begin{bmatrix} 0 \\ 1 \end{bmatrix}$, and defining the positive definite matrices $\mathbf{Q} = \begin{bmatrix} 10^3 & 0 \\ 0 & 10^3 \end{bmatrix}$, and $\mathbf{R} = \begin{bmatrix} 10^{-5} \end{bmatrix}$ the optimal solution of the feedback regulator problem is assured, and the system of Eq. 14 is asymptotically stable (Mracek and Cloutier 1998).

5.2 TDF Control Design

This control method has been successfully applied to various experimental systems including AFM problems (Yamasue and Hikihara 2006). Originally proposed by Pyragas (2002), the continuous control input $u(t, \tau)$ stabilyze the chaotic oscillation through the feedback of the difference between the current time and previous time outputs (Pyragas 2002; Yamasue and Hikihara 2006):

$$u = K [g(x_1(t - \tau), x_2(t - \tau)) - g(x_1(t), x_2(t))] \tag{18}$$

where τ is the time delay and K is the feedback gain.

The terms $g(x_1(t - \tau), x_2(t - \tau))$ and $g(x_1(t), x_2(t))$ represent scalar output signals measured at the current time t and at the previous time $t - \tau$. Since the control input (Eq. 18) only depends on the output signal the time delay τ is automatically adjusted to the period of a periodic orbit. Therefore, the control input converges to zero after the stabilization of the controlled system.

5.3 Implentation of the SDRE Method

In this work the SDRE is used in two different situations but the formulation is the same. Firstly, the SDRE is designed in order to force the chaotic system (Eq. 2) to the periodic solution obtained by the HBM (Eq. 8). The simulation result is shown in Fig. 7. Figure 7a presents the error between the

actual orbit and the desired orbit. Figure 7b, c show the controlled and uncontrolled system's response.

In Fig. 7a it can be seen that the error is max $|x - x^*| = 0.000015$ for $t \le 100$, and can be reduced by adjusting the weighting matrices $\mathbf{Q}$ and $\mathbf{R}$ in the LQR control. The controlled system is globally stable, and the proposed control method showed to be effective.

5.3.1 Synchronization Between the Systems with Chaotic and Periodic Motion

The main idea is to consider the periodic system as the master and the chaotic system as the slave, and design the SDRE control system in order to synchronize the slave system to the master system. In Fig. 8 the synchronization of the master and slave systems is shown.

The application of the control method showed to be efficient, synchronizing the slave system to the master system, with error max $|x - x^*| = 0.0003$ for $t \le 100$.

5.4 Application of TDFC Method

This section presents the application of TDFC method in the system of Eq. 2. Assuming that the oscillation velocity of Eq. 2 can be measured. The control signal is given by:

$$u = K [x_2(t - \tau) - x_2(t)] \tag{19}$$

The control signal (Eq. 19) is applied to the system of Eq. 2, resulting that:

$$\dot{x}_1 = x_2$$
$$\dot{x}_2 = d_1 x_2 + x_1 - B_1 - \frac{C_{11} + C_{12}(1 - x_1 - \eta \sin(\Omega t))^6}{(1 - y - \eta \sin(\Omega t))^8}$$
$$+ \eta \Omega^2 E_1 \sin(\omega t) + K [x_2(t - \tau) - x_2(t)] \tag{20}$$

The time delay τ and the feedback gain K are important control parameters that strongly affects the control performance. The time delay $\tau = \frac{2\pi}{\Omega}$ is used to stabilize an orbit with the same frequency of the microcantilever external excitation. According to Pyragas (2002), the feedback gain may adjusted to $K = 0.2$. Next, simulations show the application of the TDFC in the chaotic system. As it can be seen, the control method showed to be efficient in the task of keeping the system controlled Fig. 9.

6 Conclusions

In this work the microcantilever of the TM-AFM control system is modelled as an Euler–Bernoulli beam, and the tip-sample interaction forces are described by Lennard-Jones potentials. The nonlinear partial diferential equations are
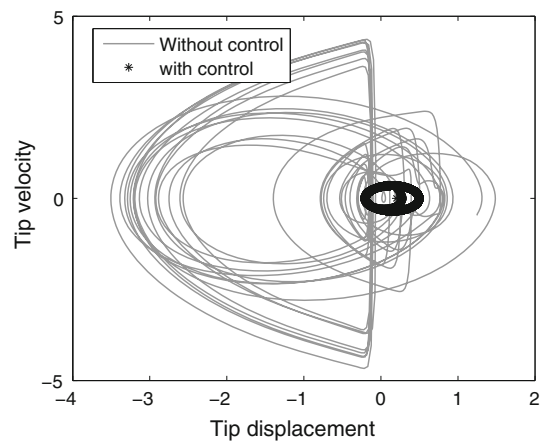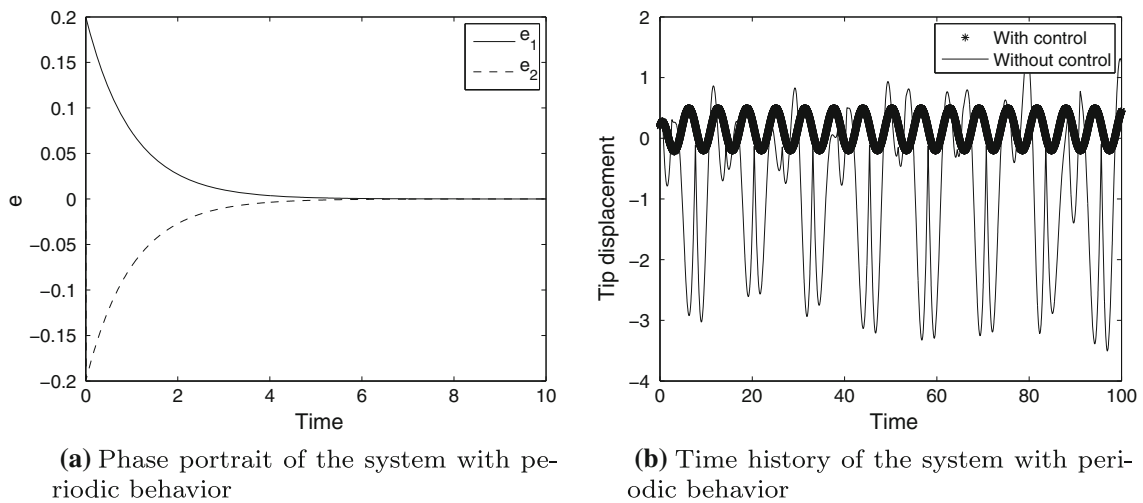
(a) Phase portrait of the system with periodic behavior

(b) Time history of the system with periodic behavior

(c) Phase portrait of the controlled and of the uncontrolled systems

Fig. 7 SDRE implementation simulation results

(a) Synchronization of master and slave systems

(b) Phase portrait of two systems, master and slave controlled
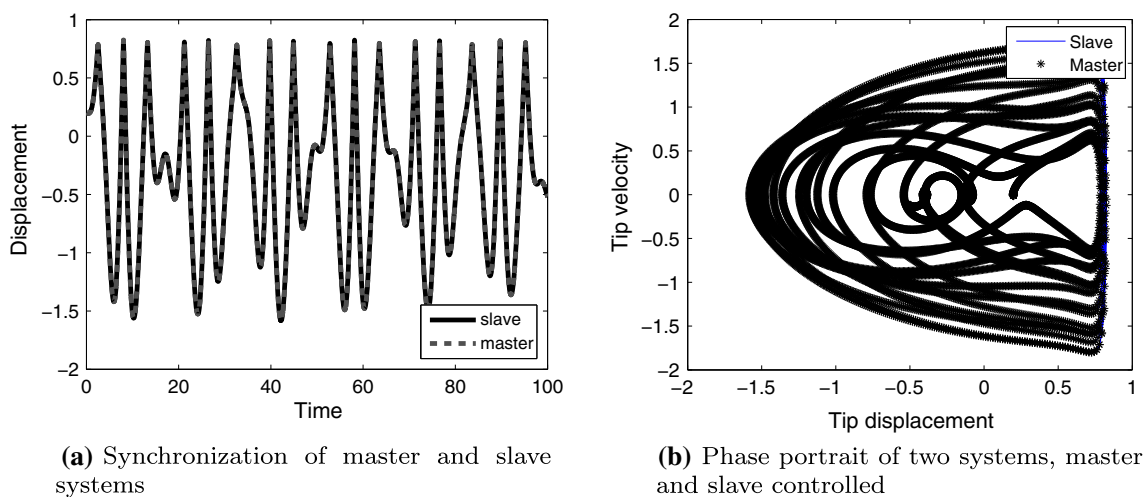
Fig. 8 Master and slave synchronization

(a) Displacement of the system with and without control

(b) Phase portrait of with and without the application of the control method
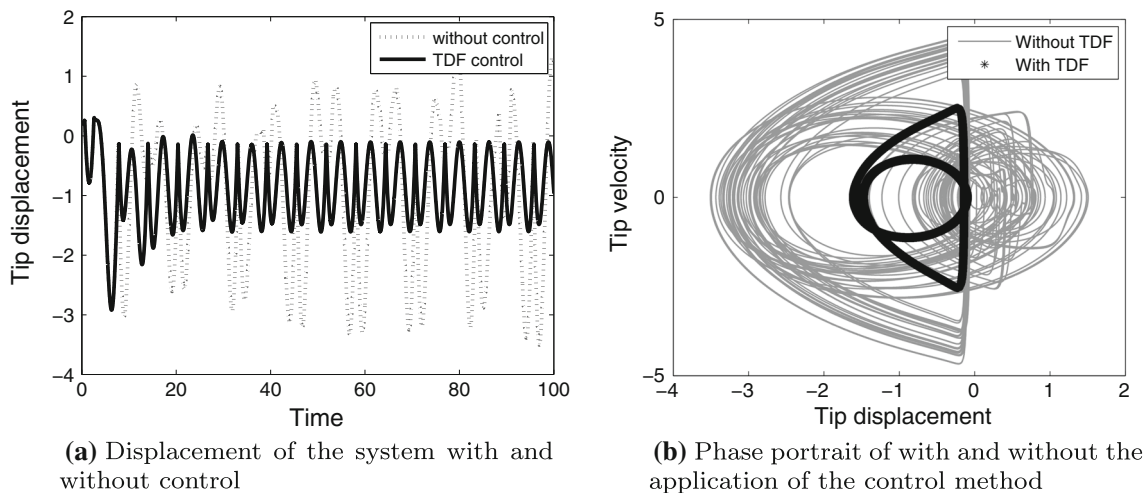
Fig. 9 TDF control implementation

truncated and only the first term of the Galerking aproximation is considered. Simulations have shown the existence of chaotic behavior by means of Lyapunov exponents, frequency spectrum, phase plots and Poincaré section plots. Aditionally, the SDRE and the TDFC techniques have been used in order to prevent the microcantiler chaotic motion. The SDRE control system has been effective in forcing the TM-AFM to the periodic orbit obtained with the HBM, and in keeping the error well damped. Also, the TDFC has been efficient, forcing the microcantiler to a periodic motion and keeping the system stable. The main advantage of the SDRE method, is the possibility of arbitrarily choose the desired periodic orbit, which is not possible for the TDFC. On the other hand, the TDFC implementation is very simple, basically depending on the choice of the time delay τ.

References

Astakhov, V., Anishchenko, V., Kapitaniak, T., & Shabunin, A. (1997). Synchronization of chaotic oscillators by periodic parametric perturbations. *Physica D: Nonlinear Phenomena*, *109*(1—–2), 11–16. Proceedings of the Workshop on Physics and Dynamics between Chaos, Order, and Noise.

Babahosseini, H., Mahboobi, S. H., & Meghdari, A. (2009). Dynamics modeling of nanoparticle in afm-based manipulation using two nanoscale friction models. In *ASME 2009 International Mechanical Engineering Congress and Exposition* (vol. 12, pp. 225–234). Micro and Nano Systems, Parts A and B.

Balthazar, J. M., Tusset, A. M., de Souza, S. L. T., & Bueno, A. M. (2013). Microcantilever chaotic motion suppression in tapping mode atomic force microscope. *Proceedings of the Institution of Mechanical Engineers, Part C: Journal of Mechanical Engineering Science*, *227*(8), 1730–1741.

Bhushan, B. (2004). *Springer handbook of nanotechnology*. Berlin: Springer.

Blazejczyk-Okolewska, B., Brindley, J., Czolczynski, K., & Kapitaniak, T. (2001). Antiphase synchronization of chaos by noncontinuous coupling: Two impacting oscillators. *Chaos, Solitons & Fractals*, *12*(10), 1823–1826.

Chua, L. O., Yang, T., Zhong, G.-Q., & Wu, C. W. (1996). Adaptive synchronization of chua's oscillators. *International Journal of Bifurcation and Chaos*, *06*(01), 189–201.

Fang, J.-Q., Hong, Y., & Chen, G. (1999). Switching manifold approach to chaos synchronization. *Physical Review E*, *59*, R2523–R2526.

Fenili, A., & Balthazar, J. M. (2011). The rigid-flexible nonlinear robotic manipulator: Modeling and control. *Communications in Nonlinear Science and Numerical Simulation*, *16*(5), 2332–2341. Biological and Mechanical Systems in Modern Control Theory DSTA2009 Conference.

Guran, A., & Rand, R. (1997). *Nonlinear dynamics: The Richard Rand 50th anniversary volume B*. Singapore: World Scientific.

Haeri, M., & Khademian, B. (2006). Comparison between different synchronization methods of identical chaotic systems. *Chaos, Solitons & Fractals*, *29*(4), 1002–1022.

Hu, S., & Raman, A. (2006). Chaos in atomic force microscopy. *Physical Review Letters*, *96*(3), 036107.

Hu, Q.-Q., & Chen, L.-Q. (2008). Bifurcation and chaos of atomic-force-microscope probes driven in Lennard-Jones potentials. *Chaos, Solitons & Fractals*, *36*(3), 740–745.

Jalili, N., & Laxminarayana, K. (2004). A review of atomic force microscopy imaging systems: Application to molecular metrology and biological sciences. *Mechatronics*, *14*(8), 907–945.

Lian, K.-Y., Liu, P., Chiang, T.-S., & Chiu, C.-S. (2002). Adaptive synchronization design for chaotic systems via a scalar driving signal. *IEEE Transactions on Circuits and Systems I: Fundamental Theory and Applications*, *49*(1), 17–27.

Liao, T. L. (1998). Adaptive synchronization of two lorenz systems. *Chaos, Solitons & Fractals*, *9*(9), 1555–1561.

Lü, J., & Zhang, S. (2001). Controlling chen's chaotic attractor using backstepping design based on parameters identification. *Physics Letters A*, *286*(2–3), 148–152.

Misra, S., Dankowicz, H., & Paul, M. R. (2008). Event-driven feedback tracking and control of tapping-mode atomic force microscopy. *Proceedings of the Royal Society A: Mathematical, Physical and Engineering Science*, *464*(2096), 2113–2133.

Morita, S., Wiesendanger, R., Meyer, E., & Giessibl, F. J. (2009). *Non-contact atomic force microscopy*. Berlin: Springer.

Mracek, C. P., & Cloutier, J. R. (1998). Control designs for the nonlinear benchmark problem via the state-dependent riccati equation method. *International Journal of Robust and Nonlinear Control*, 8(4–5), 401–433.

Nayfeh, A. H., & Mook, D. T. (1995). *Nonlinear oscillators* (1st ed.). New York: Wiley Classic Library.

Nozaki, R., Balthazar, J. M., Tusset, A. M., de Pontes, B. R, Jr, & Bueno, A. M. (2013). Nonlinear control system applied to atomic force microscope including parametric errors. *Journal of Control Automation and Electrical Systems*, 24(3), 223–231.

Pyragas, K. (2002). Analytical properties and optimization of time-delayed feedback control. *Physical Review E*, 66, 026207.

Rützel, S., Lee, S. I., & Raman, A. (2003). Nonlinear dynamics of atomic-force-microscope probes driven in Lennard-Jones potentials. *Proceedings of the Royal Society of London. Series A: Mathematical, Physical and Engineering Sciences*, 459(2036), 1925–1948.

Shawky, A. M., Ordys, A. W., Petropoulakis, L., & Grimble, M. J. (2007). Position control of flexible manipulator using non-linear H∞ with state-dependent Riccati equation. *Proceedings of the Institution of Mechanical Engineers, Part I: Journal of Systems and Control Engineering*, 221(3), 475–486.

Stark, R. W., Schitter, G., Stark, M., Guckenberger, R., & Stemmer, A. (2004). State-space model of freely vibrating and surface-coupled cantilever dynamics in atomic force microscopy. *Physical Review B*, 69, 085412.

Suykens, J. A. K., Curran, P. F., Vandewalle, J., & Chua, L. O. (1997). Robust nonlinear H∞ synchronization of chaotic Lur'e systems. *IEEE Transactions on Circuits and Systems I: Fundamental Theory and Applications*, 44(10), 891–904.

Tusset, A. M., Bueno, A. M., Nascimento, C. B., dos Santos Kaster, M., & Balthazar, J. M. (2013). Nonlinear state estimation and control for chaos suppression in mems resonator. *Shock and Vibration*, 20(4), 749–761.

Wang, C., & Ge, S. (2001). Adaptive synchronization of uncertain chaotic systems via backstepping design. *Chaos, Solitons & Fractals*, 12(7), 1199–1206.

Wang, Y., Guan, Z.-H., & Wen, X. (2004). Adaptive synchronization for chen chaotic system with fully unknown parameters. *Chaos, Solitons & Fractals*, 19(4), 899–903.

Wolf, A., Swift, J. B., Swinney, H. L., & Vastano, J. A. (1985). Determining Lyapunov exponents from a time series. *Physica D: Nonlinear Phenomena*, 16(3), 285–317.

Wu, C. W., Yang, T., & Chua, L. O. (1996). On adaptive synchronization and control of nonlinear dynamical systems. *International Journal of Bifurcation and Chaos*, 06(03), 455–471.

Yamasue, K., & Hikihara, T. (2006). Control of microcantilevers in dynamic force microscopy using time delayed feedback. *Review of Scientific Instruments*, 77(5), 053703.

Yang, X. S., Duan, C., & Liao, X. (1999). A note on mathematical aspects of drive-response type synchronization. *Chaos, Solitons & Fractals*, 10(9), 1457–1462.

Yin, X., Ren, Y., & Shan, X. (2002). Synchronization of discrete spatiotemporal chaos by using variable structure control. *Chaos, Solitons & Fractals*, 14(7), 1077–1082.

Yu, X., & Song, Y. (2001). Chaos synchronization via controlling partial state of chaotic systems. *International Journal of Bifurcation and Chaos*, 11(06), 1737–1741.

Zhao, X., & Dankowicz, H. (2006). Characterization of intermittent contact in tapping-mode atomic force microscopy. *Journal of Computational and Nonlinear Dynamics*, 1(2), 109–115.

Zhong, Q., Inniss, D., Kjoller, K., & Elings, V. (1993). Fractured polymer/silica fiber surface studied by tapping mode atomic force microscopy. *Surface Science Letters*, 290(1–2), L688–L692.